Formation of Graphene–Silicon Junction by Room Temperature Reduction With Simultaneous Defects Removal

Haokun Yi, Jun Zhao, Yuyan Huang, Guodong Zhu, Yongfeng Mei, *Member, IEEE*,
Zhuo Li, *Member, IEEE*, and Liyi Li, *Member, IEEE*

***Abstract*—A novel method of preparing reduced graphene oxide (rGO)–silicon (Si) junctions free from native silicon oxide layer at room temperature is reported. The method is based on a simultaneous reduction–dissolution reaction between graphene oxide (GO) and fresh Si atoms with the assistance of dilute hydrofluoric acid (HF). The rGO–Si junction is characterized by scanning electron microscopy, X-ray photoelectron spectroscopy, and atomic force microscopy. A reaction mechanism is proposed that Si is oxidized and dissolved by HF, which transfers the electronic holes to GO and facilitates the removal of its oxygen-containing groups. The use of HF provides a unique benefit to the contact formation that native oxide on Si is removed by HF instantaneously and only fresh Si surface is in contact with rGO. Therefore, the method provides a new strategy of preparing rGO-native oxide-free Si interface, which has been a fundamental challenge in the fabrication of graphene–Si junction. Electrical tests show that rGO–Si interface has a slightly higher barrier than Al–Si.**

***Index Terms*—2-D materials, graphene oxide (GO) reduction, graphene–silicon junction.**

I. INTRODUCTION

GRAPHENE is a 2-D nano sheet of sp^2-hybridized carbon atoms. Due to its high electron mobility and high electric current-carrying capacity, graphene has been considered as a promising microelectronic material [1], [2]. Silicon, on the other hand, is a dominant semiconductor in major microelectronic devices. Therefore, the junction between graphene and silicon (Si) has been considered as a basic building block for graphene electronics and has been intensively studied [3], [4]. Potential applications in field-effect transistors [5], solar cells [6], photodetectors [7], and gas sensors [8] have been demonstrated. Graphene–silicon Schottky junctions have shown high sensitivity to visible and IR broadband light [9], which could also be expanded to applications in biosensing [10]. The performance could be further developed by adopting more complicated topology of Si substrate, such as Si nanowires [11]. Electronic and optoelectronic properties of such junctions with controlled number of graphene layers have been studied in depth [12]. Until now, methods for fabrication of graphene–Si junctions can be categorized into the following:

1) growing graphene on Si using sacrificial catalysts from gas precursor [13];
2) direct transfer of graphene onto bare Si surface [14];
3) reduction of graphene oxide (GO) on Si [15].

Route 1 generally requires high-temperature processes which may bring integration issues if other electronic devices are present on Si. While route 2 allows room temperature process, patterning the graphene into microscopic features is difficult. For route 3, the reduction of GO typically needs external assistance, such as thermal treatment [16], hydrothermal chemical reactions [17], electrical field [15], or laser irradiation [18]. However, one fundamental limitation to form ideal graphene–Si junction in the above routes is the instantaneous formation of Si surface oxide in open air [19]. The inevitable incorporation of surface oxide between graphene and Si has negatively affected the performance of the junction [20]. This calls for a new method that can remove the oxide layer simultaneously during the contact formation, which has been a fundamental challenge in the fabrication of graphene–Si junction previously.

On the other hand, reduction of GO on fresh metal surface at ambient temperatures has been reported recently [21]–[25]. During the reduction, the metal is kept in acidic GO solution to prevent the formation of surface oxide. The metal serves as the reducing agent by itself to transform GO into reduced GO (rGO). A rGO layer on fresh metal is thus formed. In analogy, from the perspective of thermodynamics, it is feasible to use Si to reduce GO in a similar manner, given that Si has more negative reduction potential. However, the thin layer of native oxide on surface makes Si practically inert. As a

Manuscript received October 14, 2020; revised November 27, 2020; accepted December 9, 2020. Date of publication December 29, 2020; date of current version January 22, 2021. This work was supported in part by National Key Research and Development Program of China under Grant 2017YFA0204600 and 2017ZX02315005, in part by National Science Foundation of China under Grant 51703032, and in part by Shanghai Rising Star Program under Grant 20QA1401300. The review of this article was arranged by Editor F. Schwierz. *(Haokun Yi and Jun Zhao are contributed equally to this work.) (Corresponding author: Liyi Li.)*

Haokun Yi, Jun Zhao, Yuyan Huang, Guodong Zhu, Yongfeng Mei, and Zhuo Li are with the Department of Materials Science, Fudan University, Shanghai 200433, China.

Liyi Li is with the School of Electronic Science and Engineering, Southeast University, Nanjing 211189, China (e-mail: leelill1989@gmail.com).

Color versions of one or more figures in this article are available at https://doi.org/10.1109/TED.2020.3044558.

Digital Object Identifier 10.1109/TED.2020.3044558

result, successful direct reduction of GO by Si has not been reported so far. Here, we created a new method which enables such reduction by adding hydrofluoric acid (HF) in the GO solution. HF is a weak acid yet effective in removing native oxide instantaneously. The reduction potential of Si with the presence of HF in aqueous solution is more negative compared with most of the metals [26]

$$\mathrm{SiF_6^{2-}} + 4\mathrm{e} \leftrightarrow \mathrm{Si} + 6\mathrm{F^-},\ E^\circ = -1.24\ \mathrm{V}$$
$$\text{(versus standard hydrogen electrode, 298.15 K).}$$

It is conceivable that GO can be continuously reduced on oxide-free "fresh" Si surface with the assistance of HF. The generated rGO–silicon junction from direct contact and reaction is therefore a "pure" junction free from native oxide or airborne contamination, which will be beneficial for studying the junction behavior between rGO and Si and fabricating new devices based on these junctions.

II. MATERIALS AND METHODS

GO aqueous solution was provided by the Shaanxi Coal Chemical Research Institute, Chinese Academy of Science, synthesized by the modified Hummers oxidation method. The (100)-oriented single-crystalline phosphorus-doped Si wafer was cut into 1×1 cm^2 coupons and cleaned with deionized (DI) water, piranha solution, and DI water successively. The resistivity of Si is $>2000\ \Omega\cdot$cm unless described otherwise. The coupons were then dried with N_2 gas. After cleaning, the coupons were immersed directly in the mixture solution of GO and HF (aq) for various time. The concentrations of GO (c(GO)) and that of HF (c(HF)) are 5 mg/mL and 0.1 mol/L, respectively. During the reaction, the solution was stirred constantly at room temperature. After the reaction was completed, the Si coupons were rinsed by copious DI water before drying with N_2 gas. The polished side and the nonpolished side of the Si substrates are referred to as the frontside and the backside, respectively. During the deposition of GO, the backside was sealed hermetically from contacting the GO solution, so that the GO is only deposited on the frontside of Si substrates.

The morphology of the GO-HF samples was characterized by field emission scanning electron microscopy (SEM) (JEOL JSM-6701F). X-ray photoelectron spectroscopy (XPS) measurements were carried out using a Kratos Axis Ultra delay-line detector (DLD) X-ray photoelectron spectrometer with a monochromatic Al target, and the total spectral pass was 160 eV. Raman spectra were captured at room temperature on the Horiba HR800 confocal microscopic with a Raman spectrometer using Ar laser (514 nm). Atom force microscope (AFM) images were captured by a Bruker Dimension Edge AFM.

The current–voltage (I–V) curves of the GO-HF samples with 5-min deposition time were measured by Keithley 4200 source meter at a temperature of 298 K. The current was recorded with constant voltage sweep rate of 0.05 V/step. Tungsten probes with 0.2-μm nominal tip diameter were used to make contact on the top surface of coupons. A layer of Al thin film with a nominal thickness of 50 nm was coated on both the sides using a Kurt Lesker PVD75 sputter coater. Control samples were made by coating Al using the same method on both the sides of bare Si substrates. All edges of the samples were protected by Kapton tape before Al deposition to avoid leakage current passing through the Al on the edges.

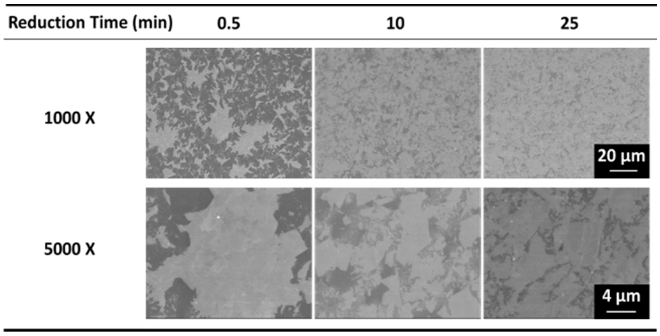

Fig. 1. Top–down SEM images of GO reduced on Si with reduction time of 0.5, 10, and 25 min at magnification of 1000× and 5000×, respectively.

III. RESULTS

Si test coupons ((100)-oriented single-crystalline phosphorus-doped Si, 1 cm × 1 cm) with resistivity above 2000 $\Omega\cdot$cm was immersed in the mixture aqueous solution of GO (5 mg/mL) and HF (0.1 mol/L) for various time. During the immersion, the solution was stirred constantly at room temperature. After taking out from the solution, the coupons were rinsed by copious DI water before drying with N_2 gas. The Si coupons with immersion time of 0.5, 10, and 25 min are referred to as GO-HF (0.5), GO-HF (10), and GO-HF (25), respectively. As shown in Fig. 1, densely packed flakes can be observed on the Si surface of these GO-HF samples from the top–down SEM images. Based on the morphology, the flakes should be either GO or their chemically reduced form, rGO. Fig. 1 also illustrates that as the reduction time increases, the surface coverage of the flakes on Si also grows. Under higher magnification, the boundary between flakes or the wrinkles within flakes becomes less well-defined, indicating a higher thickness of the flake stacks. An image contrast analysis gives an estimate surface coverage of 47%, 75%, and 94% at reduction time of 0.5, 10, and 25 min, respectively. The gradual increase in surface coverage indicates that there might be slow reactions between GO and Si as the Si coupons were immersed in the GO-HF solution. To illustrate the effect of HF, a control sample was prepared by immersing the Si coupon in the same GO solution without HF at room temperature and subsequently rinsed and dried in the same manner. The control sample is referred to as GO-Si. While the flakes in the GO-HF samples survived multiple water rinse, the flakes in GO-Si completely disappeared from Si surface under the same operation. The increased adhesion between the flakes and Si in the GO-HF samples after copious water rinsing suggests a difference in the chemistry to GO.

The flakes in the GO-HF and pristine GO were further characterized by Raman spectroscopy and XPS to confirm their chemical difference. As shown in Fig. 2(a), both GO and GO-HF (0.5) show clear D peak at 1344 cm^{-1} and G

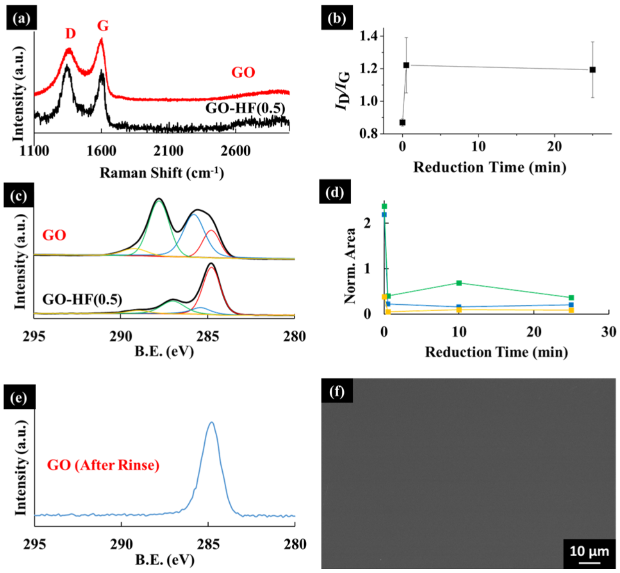

Fig. 2. (a) Raman spectra of GO and rGO on Si. (b) Plot of I_D/I_G in the Raman spectra of rGO versus reduction time. (c) High-resolution C1s XPS spectra of GO and rGO on Si. The raw data curves (black—) are deconvoluted into peaks of -C = C-/-C-C- (red—), -C-O- (blue—), -C = O (green—), and -C(= O)-O (yellow—). (d) Plot of deconvoluted C1s XPS peak area of GO versus reduction time. The areas of -C-O- (blue—), -C = O (green—), and -C(= O)-O (yellow—) are all normalized to that of -C = C-/-C-C- illustrated in (c). (e) XPS spectrum of GO after water rinse. (f) SEM image of GO after water rinse.

peak at 1590 cm^{-1}. The ratio of intensity of the two peaks, I_D/I_G, is calculated from Raman spectra taken from over four spots per sample. The average of I_D/I_G values are 0.9 and 1.2 for GO and GO-HF (0.5), respectively. The GO sample is considered as of reduction time of 0 min. I_D/I_G stays relatively constant for GO-HF with longer reduction time [Fig. 2(b)]. The increase in I_D/I_G in GO-HF samples versus GO sample is similar to the hydrothermal reduction of GO previously reported [17], [27], which could be explained by a decreased average area of sp^2-hybridized planes after reduction [28]. Fig. 2(c) shows high-resolution C1s XPS spectra of GO and GO-HF (0.5). The raw peak is deconvoluted into peaks of C-C/C = C at 284.5 eV, C-O at 285.4 eV, C = O at 287.13 eV, and carboxyl group (-COOH at 288.95 eV) [29].The area of all the peaks of the oxygen-containing groups (O groups) are normalized to that of the C-C/C = C peak. Fig. 2(d) plots the normalized peak area of the GO-HF samples at different reduction time. Similar to the result of Raman spectroscopy in Fig. 2(b), the normalized area of the O-related groups drops sharply from GO to GO-HF (0.5) while does not change significantly over reduction time up to 25 min. XPS of the GO-Si control sample only shows the signal of airborne hydrocarbon [Fig. 2(e)], consistent with the SEM images that show no GO remains on Si substrate after water rinse [Fig. 2(f)]. The data in Fig. 2 support the model that the flakes in the GO-HF samples are rGO. Considering the results in Fig. 1, it can be inferred that more GO flakes are reduced on Si surface with longer reduction time. Therefore, the rGO stack thickness can be controlled by the reduction time.

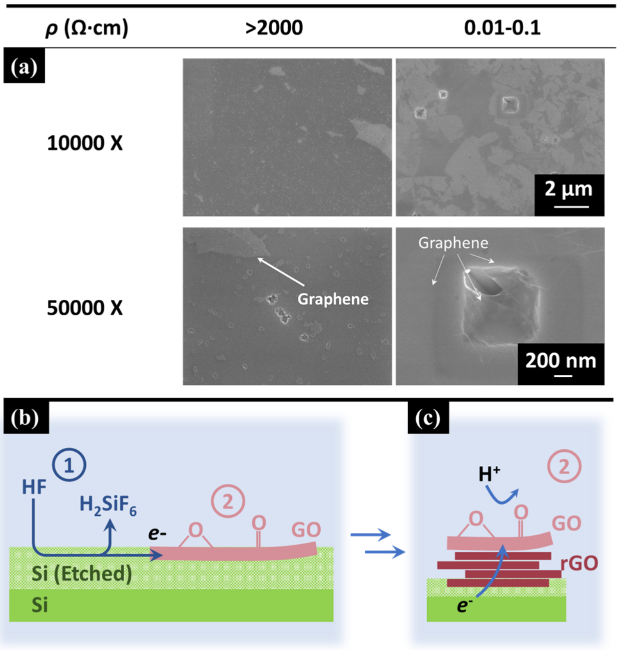

Fig. 3. (a) Top–down SEM images of GO-HF samples on Si with resistivity of >2000 Ω·cm (left column) and 0.01–0.1 Ω·cm (right column) in mixture solution of 5 mg/mL GO and 4 mol/L HF for 25 min. (b) and (c) Proposed reaction mechanism of Si in GO-HF solution. Anodic etching of Si and electrochemical reduction of GO are labeled as process 1 and 2, respectively.

IV. DISCUSSION

To further elucidate the reduction mechanism of GO in the GO-HF samples, reduction reactions were carried out using solution with much higher HF concentration ($c(\mathrm{HF}) = 4$ mol/L). Notably, pores on the surface of can be observed in Fig. 3(a), while the surface of Si etched by lower $c(\mathrm{HF})$ in Fig. 1 is smooth without pores. Especially, if Si coupons with lower resistivity of 0.01–0.1 Ω·cm are used, the size of the pores increases compared with those on the Si of >2000 Ω·cm. The top–down SEM images of 50 000× magnification in Fig. 3 reveal an interesting phenomenon that the rGO flakes are overhanging on the pores, rather than conforming to the sidewall profile of the pores. Given the fact that no pores are observed on the Si coupons before reaction, the pores should be generated during the reduction reaction of GO. Considering an etch rate of 30 nm/min that is estimated from the size of the pores in Fig. 3(a), the etch rate is too large to be caused by pure HF etching on Si [30].In fact, the dependence of Si surface morphology on $c(\mathrm{HF})$ or ρ_{Si} is a typical feature of electrochemical etching (ECE) of Si [31]. During the ECE, Si is electrochemically oxidized by electronic holes (h^+) and dissolved by HF. Depending on the relative amount of h^+ and HF, the ECE reaction can follow two different routes:

Electropolishing (EP)

$$\mathrm{Si} + x\mathrm{H_2O} + 2x\mathrm{h}^+ \rightarrow \mathrm{SiO}_x + 2x\mathrm{H}^+ \qquad (1)$$

$$\mathrm{SiO}_x + 6\mathrm{HF} + (4-2x)\mathrm{h}^+ \rightarrow \mathrm{H_2SiF_6} + x\mathrm{H_2O} + (4-2x)\mathrm{H}^+. \qquad (2)$$

Pore-formation (PF)

$$\mathrm{Si} + 6\mathrm{HF} + 4\mathrm{h}^+ \rightarrow 4\mathrm{H}^+ + \mathrm{H_2SiF_6}. \quad (3)$$

In the EP-type ECE, the supply of h^+ overwhelms that of HF, and therefore, the surface layer of Si atoms is oxidized to suboxides layer, SiO_x. This layer is then slowly dissolved by HF. Since the oxidation of Si and the subsequent dissolution is relatively isotropic, the EP-type ECE results in a smooth surface. On the contrary, in the PF-type ECE, the supply of h^+ is deficient and tends to be concentrated at regions with high surface curvature, which facilitates growth of pores. In other words, the surface roughness of Si after ECE increases with c(HF) at a given h^+ supply rate. On the other hand, PF is favored as ρ_{Si} decreases due to a lower breakdown voltage [32]. The trend has been demonstrated not only in ECE where h^+ are supplied by an electrical source but also in similar Si chemical etching systems where h^+ are generated by cathodic reactions, such as those in HNO_3-HF etching [33] and H_2O_2-HF-based metal-assisted chemical etching [34].

Given the similar dependence of Si surface morphology on ρ_{Si} and c(HF) shown in the GO-HF system, we propose a mechanism that GO is an oxidant and directly reduced by Si through electrochemical reactions in (1)–(3). The overall reaction can be written as

$$\mathrm{GO} + \mathrm{HF} + \mathrm{Si} \rightarrow \mathrm{rGO} + \mathrm{H_2SiF_6} + \mathrm{H_2O}. \quad (4)$$

The reaction is thermodynamically favorable according to the standard reduction potential of relevant half reactions [21], [26]

$$\mathrm{SiF_6^{2-}} + 4\mathrm{e} \Longleftrightarrow \mathrm{Si} + 6\mathrm{F}^-, \quad E = -1.24\ \mathrm{V}$$
$$\text{versus standard hydrogen electrode} \quad (5)$$
$$\mathrm{GO} + H^+ \Longleftrightarrow \mathrm{rGO}, \quad E = 0.4 - 0.6\ \mathrm{V(pH = 6.0)}. \quad (6)$$

Consistent with the trend of ECE, pores are generated at a high c(HF) and a low ρ_{Si} in Fig. 3. At lower c(HF) and higher ρ_{Si}, Si is dissolved while remaining a smooth top surface, which shows no pores under SEM in Fig. 1. Furthermore, ECE can induce the etching of Si that is not in direct contact with the oxidant, since the surface of Si can redistribute electrochemical potential [35]. This explains that the GO in the bottom right image of Fig. 3(a) is not conforming to the sidewall of the pore. During the reaction, the first layer of GO that is reduced on Si should keep close to Si under attractive forces. Attractive van der Waals forces have been discovered between Au and Si during similar HF-based etching reactions [36], [37]. This attractive force also explains the increased adhesion between rGO flakes and Si that can resist copious water rinse in Fig. 1. As the reaction proceeds, the rGO layers pass electrons from Si to more GO flakes in solution. Stacks of rGO are thus formed. In other words, the upper layers of GO in the stacks are also chemically reduced, although not in direct contact of Si surface [Fig. 3(c)]. This mechanism indicates the fundamental viability of forming multilayer rGO film on Si using this method. This aspect is also supported by the Raman [Fig. 2(b)] and XPS data [Fig. 2(d)] that across the reaction of 25 min, the spectra remain characteristic of rGO rather than GO while the number of rGO layers keeps increasing.

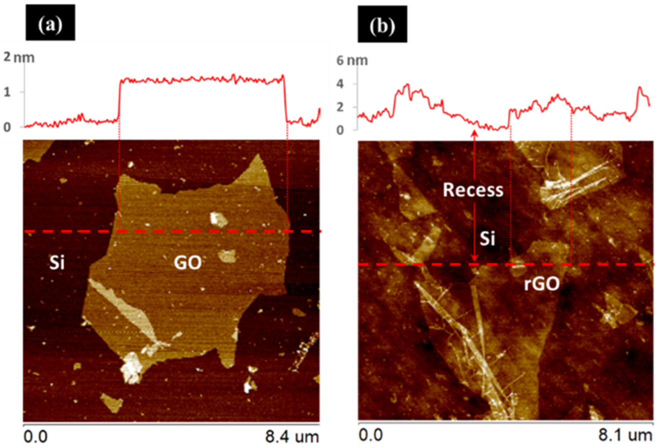

Fig. 4. AFM height images of (a) GO and (b) rGO on Si surface. The concentration of GO in the solution is diluted to 0.025 mg/mL to enable the measurement of individual GO. For the rGO shown in (b), the deposition time is 0.5 min. Height profile along the red dash lines is shown on top of each image.

Fig. 4(a) and (b) shows the AFM images of GO and rGO. The samples used for AFM studies were prepared by dispensing diluted GO (0.025 mg/mL) solution on cleaned wafer for the GO sample and GO-HF (0.5) for the rGO sample. The cross-sectional view of the thickness of the single GO sheet is 1.1–1.3 nm. For the rGO sample, some recess regions with depth of 1–2 nm can be observed from the surface profile. The surface recess supports the model that Si is dissolved during deposition of rGO; its magnitude of 1–2 nm suggests an EP-type ECE.

The electrical property of the rGO is evaluated by measuring the I–V curve of the GO-HF (10) samples (referred to as rGO-Si sample). A control sample in which the aluminum (Al) film is deposited on the frontside of the bare Si surface is fabricated as a benchmark. Al film is also deposited on the backside of Si substrates for both the samples as electrical contact layer. The schematic close circuits of both the samples are shown in Fig. 5(a) and (b), respectively. The I–V curves collected from such circuits are shown in Fig. 5(c). To understand the electrical property of the rGO–Si interface, both the circuits are modeled by a back-to-back double Schottky junction [Fig. 5(d)] [38], where both the surfaces of Si substrates are considered as Schottky diodes. Since the Si backside is not polished and much rougher than the frontside surface, the backside Al–Si interface is assumed to have a higher barrier for electron transport. Based on the shape of the I–V curves, the frontside surface is considered as under reverse bias when $V > 0$. Therefore, the I–V curves can be modeled by

$$I = I_s \exp\left(-\frac{V - IR}{\eta k_B T}\right)\left[\exp\left(\frac{V - IR}{k_B T}\right) - 1\right] \quad (7)$$

where k_{B}, T, and η are the Boltzmann's constant, temperature, and ideality factor, respectively. R is the equivalent contact resistance of interfaces including wires to the source meter,

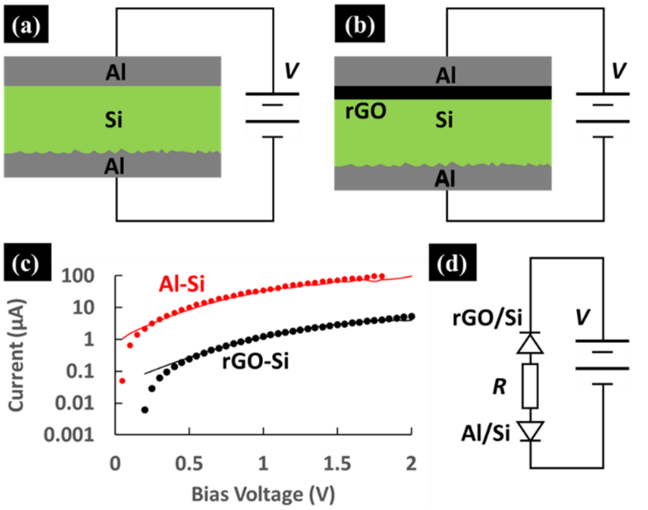

Fig. 5. Schematic circuits for electrical testing of (a) Al–Si interface as the control sample and (b) rGO–Si interface. (c) Current–voltage (*I*–*V*) curves of Al–Si (red dots) and rGO–Si (black dots) samples. The calculated curves for Al–Si and rGO–Si samples are shown in red and black solid lines, respectively, using the equivalent circuit model shown in (d) and (7).

wires to Al, Al to the backside of Si, and resistance through the Si substrates. R is estimated using the I–V curves in the highly positive voltage range (1.5–2.0 V). I_s is the saturation current of the Si frontside junction

$$I_s = A^* S T^2 \exp\left(-\frac{q\phi_B}{k_B T}\right) \tag{8}$$

where $A*$ and S are the effective Richardson constant of Si (112 $\mathrm{A{\cdot}K^{-2}{\cdot}cm^{-2}}$) and Schottky diode contact area (1 $\mathrm{cm^2}$), respectively. ϕ_B is the barrier height of the diode. As shown in Fig. 5(c), the experimental data fit the model reasonably well in the voltage range of 0.5–1.5 V. According to the results of modeling, ϕ_B of the rGO–Si interface is 0.855 V with η of 1.13. In comparison, ϕ_B of the Al–Si interface is 0.830 V with η of 1.21.

V. CONCLUSION

In summary, SEM, Raman, and XPS data confirm the reduction of GO by Si with the assistance of HF. A mechanism is proposed that Si is oxidized and dissolved by HF. Such reduction process transfers h^+ to GO and facilitates the removal of its oxygen-containing groups. Electrical tests show that rGO–Si interface has a slightly higher barrier than Al–Si. It should be noted that rGO in this article is likely to inherit defects, such as hydroxyl, carbonyl, and carboxylate groups from GO made by Hummers method. These defects generally make rGO have lower electrical conductivity and wider bandgap compared with mechanically exfoliated grapheme [39]. It has been reported that mechanically exfoliated graphene are better dissolved in nonaqueous solvent, such as N-methyl-2-pyrrolidone [40]. Reaction of such graphene on Si is to be explored to achieve Schottky junctions with extended range of graphene defects density. The successful reduction of GO by Si provides a new strategy of preparing high-quality rGO–Si interface free from native silicon oxide at room temperature. The insight may also help the fast expanding research community of 2-D nanomaterials in general.

ACKNOWLEDGMENT

The authors would like to thank Prof. Xiaosheng Fang for the useful discussion.

REFERENCES

[1] Y.-M. Lin, C. Dimitrakopoulos, K. A. Jenkins, D. B. Farmer, H.-Y. Chiu, A. Grill, and P. Avouris, "100-GHz transistors from wafer-scale epitaxial graphene," *Science*, vol. 327, no. 5966, p. 662, Feb. 2010.
[2] K. I. Bolotin *et al.*, "Ultrahigh electron mobility in suspended graphene," *Solid State Commun.*, vol. 146, nos. 9–10, pp. 351–355, Jun. 2008.
[3] C. C. Chen, M. Aykol, C. Chang, A. F. J. Levi, and S. B. Cronin, "Graphene-silicon Schottky diodes," *Nano Lett.*, vol. 11, pp. 1863–1867, Apr. 2011.
[4] D. Sinha and J. U. Lee, "Ideal graphene/silicon Schottky junction diodes," *Nano Lett.*, vol. 14, no. 8, pp. 4660–4664, Aug. 2014.
[5] J. S. Moon *et al.*, "Top-gated graphene field-effect transistors using graphene on Si (111) wafers," *IEEE Electron Device Lett.*, vol. 31, no. 11, pp. 1193–1195, Nov. 2010.
[6] G. Fan *et al.*, "Graphene/silicon nanowire Schottky junction for enhanced light harvesting," *ACS Appl. Mater. Interface*, vol. 3, no. 3, pp. 721–725, Mar. 2011.
[7] F. Liu and S. Kar, "Quantum carrier reinvestment-induced ultrahigh and broadband photocurrent responses in graphene–silicon junctions," *ACS Nano*, vol. 8, no. 10, pp. 10270–10279, Oct. 2014.
[8] J. Kim, S. D. Oh, J. H. Kim, D. H. Shin, S. Kim, and S.-H. Choi, "Graphene/Si-nanowire heterostructure molecular sensors," *Sci. Rep.*, vol. 4, no. 1, pp. 1–5, Jun. 2014.
[9] A. Hekmatikia and Y. Abdi, "Graphene–silicon-based high-sensitivity and broadband phototransistor," *IEEE Electron Device Lett.*, vol. 39, no. 2, pp. 216–219, Feb. 2018.
[10] A. A. Noroozi and Y. Abdi, "A graphene/Si Schottky diode for the highly sensitive detection of protein," *RSC Adv.*, vol. 9, no. 34, pp. 19613–19619, 2019.
[11] A. Ghadakchi and Y. Abdi, "Reduced graphene oxide/silicon nanowire heterojunction for high sensitivity and broadband photodetector," *IEEE Sensors Lett.*, vol. 3, no. 8, pp. 1–4, Aug. 2019.
[12] M. Javadi, A. Noroozi, A. Mazaheri, and Y. Abdi, "Sequentially assembled graphene layers on silicon, the role of uncertainty principles in graphene–silicon Schottky junctions," *Adv. Opt. Mater.*, vol. 7, no. 19, Oct. 2019, Art. no. 1900470.
[13] S. Naghdi, K. Y. Rhee, and S. J. Park, "Transfer-free chemical vapor deposition of graphene on silicon substrate at atmospheric pressure: A sacrificial catalyst," *Thin Solid Films*, vol. 657, pp. 55–60, Jul. 2018.
[14] J. W. Suk *et al.*, "Transfer of CVD-grown monolayer graphene onto arbitrary substrates," *ACS Nano*, vol. 5, no. 9, pp. 6916–6924, Sep. 2011.
[15] A. G. Marrani, R. Zanoni, R. Schrebler, and E. A. Dalchiele, "Toward graphene/silicon interface via controlled electrochemical reduction of graphene oxide," *J. Phys. Chem. C*, vol. 121, no. 10, pp. 5675–5683, Mar. 2017.
[16] S. Pei and H.-M. Cheng, "The reduction of graphene oxide," *Carbon*, vol. 50, no. 9, pp. 3210–3228, 2012.
[17] Z. Lin, Y. Yao, Z. Li, Y. Liu, Z. Li, and C.-P. Wong, "Solvent-assisted thermal reduction of graphite oxide," *J. Phys. Chem. C*, vol. 114, no. 35, pp. 14819–14825, Sep. 2010.
[18] V. A. Kondrashov, N. S. Struchkov, R. Y. Rozanov, V. K. Nevolin, D. S. Kopylova, and A. G. Nasibulin, "Graphene oxide reduction by solid-state laser irradiation for bolometric applications," *Nanotechnology*, vol. 29, no. 3, Jan. 2018, Art. no. 035301.
[19] S. R. Na, J. W. Suk, R. S. Ruoff, R. Huang, and K. M. Liechti, "Ultra long-range interactions between large area graphene and silicon," *ACS Nano*, vol. 8, no. 11, pp. 11234–11242, Nov. 2014.
[20] C. Bautista-Flores, R. Y. Sato-Berrú, and D. Mendoza, "Raman spectroscopy of CVD graphene during transfer process from copper to SiO_2/Si substrates," *Mater. Res. Express*, vol. 6, no. 1, Oct. 2018, Art. no. 015601.
[21] X. Cao *et al.*, "Ambient fabrication of large-area graphene films via a synchronous reduction and assembly strategy," *Adv. Mater.*, vol. 25, no. 21, pp. 2957–2962, Jun. 2013.

[22] U. N. Maiti, J. Lim, K. E. Lee, W. J. Lee, and S. O. Kim, “Three-dimensional shape engineered, interfacial gelation of reduced graphene oxide for high rate, large capacity supercapacitors,” *Adv. Mater.*, vol. 26, no. 4, pp. 615–619, Jan. 2014.

[23] B. Song, L. Li, Z. Lin, Z.-K. Wu, K.-S. Moon, and C.-P. Wong, “Water-dispersible graphene/polyaniline composites for flexible micro-supercapacitors with high energy densities,” *Nano Energy*, vol. 16, pp. 470–478, Sep. 2015.

[24] Z.-K. Wu *et al.*, “Flexible micro-supercapacitor based on *in-situ* assembled graphene on metal template at room temperature,” *Nano Energy*, vol. 10, pp. 222–228, Nov. 2014.

[25] Z. Li, W. Guo, Y. Huang, K. Zhu, H. Yi, and H. Wu, “On-skin graphene electrodes for large area electrophysiological monitoring and human-machine interfaces,” *Carbon*, vol. 164, pp. 164–170, Aug. 2020.

[26] D. R. Lide, “CRC handbook of chemistry and physics,” in *Electrochemical Series*, 84th ed. Boca Raton, FL, USA: CRC Press, 2004.

[27] S. Stankovich *et al.*, “Synthesis of graphene-based nanosheets via chemical reduction of exfoliated graphite oxide,” *Carbon*, vol. 45, no. 7, pp. 1558–1565, Jun. 2007.

[28] D. R. Dreyer, S. Park, C. W. Bielawski, and R. S. Ruoff, “The chemistry of graphene oxide,” *Chem. Soc. Rev.*, vol. 39, no. 1, pp. 228–240, 2010.

[29] L. Li *et al.*, “Molecular engineering of aromatic amine spacers for high-performance graphene-based supercapacitors,” *Nano Energy*, vol. 21, pp. 276–294, Mar. 2016.

[30] K. R. Williams, K. Gupta, and M. Wasilik, “Etch rates for micromachining processing-part II,” *J. Microelectromech. Syst.*, vol. 12, no. 6, pp. 761–778, Dec. 2003.

[31] X. G. Zhang, *Electrochemistry of Silicon and its Oxide*. New York, NY, USA: Kluwer, 2001, pp. 344–345.

[32] V. Lehmann, “The physics of macropore formation in low doped n-type silicon,” *J. Electrochem. Soc.*, vol. 140, no. 10, pp. 2836–2843, Oct. 1993.

[33] H. Robbins and B. Schwartz, “Chemical etching of silicon.1. The system Hf, HNO_3, and H_2O,” *J. Electrochem. Soc.*, vol. 106, no. 6, pp. 505–508, 1959.

[34] C. Chartier, S. Bastide, and C. Lévy-Clément, “Metal-assisted chemical etching of silicon in HF–H_2O_2,” *Electrochim. Acta*, vol. 53, no. 17, pp. 5509–5516, Jul. 2008.

[35] L. Li, X. Zhao, and C.-P. Wong, “Deep etching of single- and polycrystalline silicon with high speed, high aspect ratio, high uniformity, and 3D complexity by electric bias-attenuated metal-assisted chemical etching (EMaCE),” *ACS Appl. Mater. Interface*, vol. 6, no. 19, pp. 16782–16791, Oct. 2014.

[36] O. J. Hildreth, K. Rykaczewski, A. G. Fedorov, and C. P. Wong, “A DLVO model for catalyst motion in metal-assisted chemical etching based upon controlled out-of-plane rotational etching and force-displacement measurements,” *Nanoscale*, vol. 5, no. 3, pp. 961–970, 2013.

[37] C. Q. Lai, H. Cheng, W. K. Choi, and C. V. Thompson, “Mechanics of catalyst motion during metal assisted chemical etching of silicon,” *J. Phys. Chem. C*, vol. 117, no. 40, pp. 20802–20809, Oct. 2013.

[38] S. N. C. Azmi, S. F. A. Rahman, A. Nawabjan, and A. M. Hashim, “Junction properties analysis of silicon back-to-back Schottky diode with reduced graphene oxide Schottky electrodes,” *Microelectron. Eng.*, vol. 196, pp. 32–37, Sep. 2018.

[39] G. Eda, C. Mattevi, H. Yamaguchi, H. Kim, and M. Chhowalla, “Insulator to semimetal transition in graphene oxide,” *J. Phys. Chem. C*, vol. 113, no. 35, pp. 15768–15771, Sep. 2009.

[40] T. Skaltsas, N. Karousis, H.-J. Yan, C.-R. Wang, S. Pispas, and N. Tagmatarchis, “Graphene exfoliation in organic solvents and switching solubility in aqueous media with the aid of amphiphilic block copolymers,” *J. Mater. Chem.*, vol. 22, no. 40, pp. 21507–21512, 2012.